13th AIAA/ISSMO Multidisciplinary Analysis Optimization Conference
13 - 15 September 2010, Fort Worth, Texas

AIAA 2010-9279

Comparison of Surrogate Models Used for Adaptive Optimal Control of Active Thermoelectric Windows

Junqiang Zhang*
Rensselaer Polytechnic Institute, Troy, New York 12180

Achille Messac†
Syracuse University, Syracuse, NY, 13244

Jie Zhang*and Souma Chowdhury*
Rensselaer Polytechnic Institute, Troy, New York 12180

This paper compares the performances of standard surrogate models in the development of an optimal control framework. The optimal control strategy is implemented on an Active Thermoelectric (ATE) window design. The ATE window design uses thermoelectric units to actively regulate the overall thermodynamic properties of the windows. The optimization of the design is a multiobjective problem, where both the heat transferred through the window and electric power consumption are minimized. The power supplies and the heat transfer are optimized under a reasonable number of randomly sampled environmental conditions. The subsequent optimal designs obtained are represented as functions of the corresponding environmental conditions using surrogate models. To this end, four types of surrogate models are used, namely, (i) Quadratic Response Surface Methodology (QRSM), (ii) Radial Basis Functions (RBF), (iii) Extended Radial Basis Functions (E-RBF), and (iv) Kriging. Their performances are compared using two accuracy measurement metrics: Root Mean Squared Error (RMSE) and Maximum Absolute Error (MAE). We found that any one of the surrogate modeling methods is not superior to the others over the whole domain for the optimal control of the ATE window.

I. Introduction

In many optimization problems, system simulation requires computationally expensive simulations or analyses to evaluate the design objectives and the constraint functions. Surrogate modeling methods provide computational efficient substitution for the complex high-fidelity models.[1–3] To reduce the computational cost, the objective functions and the constraints are evaluated at a finite number of points in the design space to achieve high fidelity results. Using the high fidelity results, low fidelity surrogate models are developed to mimic the performance through the entire design space. The application of surrogate models in optimization can significantly reduce the analysis time and improve the design efficiency. Based on linear and non-linear regression and other variants of least square technique, a wide variety of surrogate modeling methods have been developed, and they are used both in academia and industry. These methods include: (*i*) Polynomial Response Surface Model[4] (*ii*) Radial Basis Functions,[5–8] (*iii*) Extended Radial Basis Functions,[9–11] (*iv*) Kriging,[12–14] (*v*) Artificial Neural Networks,[15,16] and (*vi*) Support Vector Regression.[15,17–19]

Active thermoelectric (ATE) window design is a complex multidisciplinary design that integrates thermodynamic units, fans, thermostats and sensors to passive three-pane windows.[20–24] The design is optimized

*Doctoral Student, Department of Mechanical, Aerospace and Nuclear Engineering. AIAA Student Member
†Distinguished Professor and Department Chair, Department of Mechanical and Aerospace Engineering. AIAA Lifetime Fellow. Corresponding author (messac@syr.edu)

using Matlab and Fluent to achieve both low heat transfer through ATE windows and high energy efficiencies under changing weather conditions. To represent the optimal performance of the ATE windows under varying weather conditions, surrogate models are developed to represent the optimal operations.

The ATE window design is introduced in Section II. The optimization problem of the design is formulated in Section III. In Section IV, the surrogate models of optimal operation are developed using different surrogate modeling methods. The performance of the different surrogate models are evaluated and discussed in Section V. Concluding remarks are presented in section VI.

II. The Design of Active Thermoelectric Windows

The ATE window design presented in this paper has the same structure of panes and frames as a traditional three-pane passive window. There are eight major subsystems in the ATE window: the air gap, the two side channels, the TE units, the fans, the two fins in the side channels, the heat sink, the sensors, and the thermostat. A simplified schematic of the ATE window is shown in Fig. 1.

The ATE windows are used throughout the year. The indoor temperature is assumed to be kept at a comfortable value. In this paper, heating condition is defined as: the indoor temperature is higher than the outdoor temperature, and the ATE window needs to reduce the heat transferred from inside to outside. Cooling condition is defined as: the indoor temperature is lower than the outdoor temperature, and the ATE window needs to reduce the heat transferred from outside to inside.

The ATE windows use TE units and fans to control the heat transferred through the inner panes. Each TE unit consists of thermocouples which, when supplied with electric current, induce heat flow in the direction of the current. This is known as the Peltier effect.[25] Because of the thermocouples' electrical resistance, heat is generated - the Joules effect. As the results of the two conflicting effects, heat is absorbed on the cold side and released from the hot side. Note that heating condition and cooling condition can be reversed simply by reversing the polarities of the TE units, thereby causing the current to reverse direction. The fans are used to introduce forced convection on the air flow between the inner pane and the middle pane.

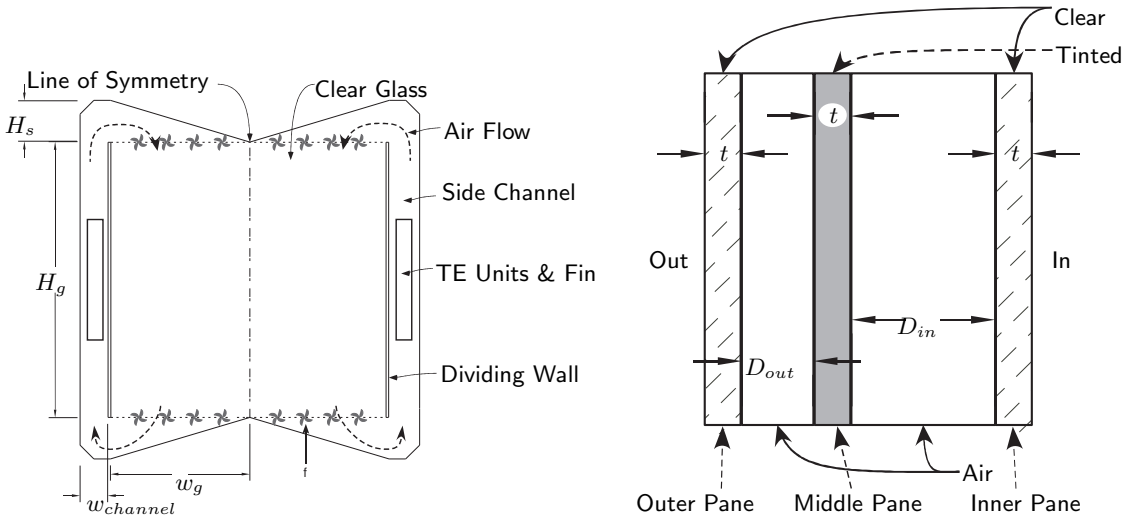

(a) Front View (b) Cross Section of Side View

Figure 1. Schematic of the ATE window

The ATE window has three panes as shown in the section view in Fig. 1(b). The air gap between the middle and outer panes is not controlled, which is same as that in a passive window. The thermodynamic properties of the air gap between the inner and middle panes are actively controlled so as to minimize the heat transfer through the inner pane. The TE units are located in the two side channels. Inside either of the left or the right side channel, there is a thin rectangular fin that is connected to the TE units to increase heat exchange between the TE units and the air flow through the channel. To reduce the thermal resistance between the outdoor environment and the TE units, heat sinks are connected to the side of TE units that interacts with the outside air. Fans are installed both on the top and the bottom of the air gap between the

inner pane and the middle pane. The air flow goes through the side channels and is heated or cooled by the fins. Figure 1(a) illustrates the air flow under heating conditions.

The sixteen fans are separated into four groups according to their locations, the top left, the top right, the bottom left, and the bottom right (see Fig. 1(a)). It is assumed that, in each group, the pressure gradient of each pan is expressed by a linear function of an average pressure gradient and a slope. The average pressure gradient, Δp_{avg}, and the slope, k, are the same for four different groups. Inside each group, the pressure gradients of the fans are expressed in Table 1.

Table 1. Pressure gradients of fans in four groups

Group	Left Most	Center Left	Center Right	Right Most
Top Left	$(1-3k)\Delta p_{avg}$	$(1-k)\Delta p_{avg}$	$(1+k)\Delta p_{avg}$	$(1+3k)\Delta p_{avg}$
Top Right	$(1+3k)\Delta p_{avg}$	$(1+k)\Delta p_{avg}$	$(1-k)\Delta p_{avg}$	$(1-3k)\Delta p_{avg}$
Bottom Left	$(1-3k)\Delta p_{avg}$	$(1-k)\Delta p_{avg}$	$(1+k)\Delta p_{avg}$	$(1+3k)\Delta p_{avg}$
Bottom Right	$(1+3k)\Delta p_{avg}$	$(1+k)\Delta p_{avg}$	$(1-k)\Delta p_{avg}$	$(1-3k)\Delta p_{avg}$

Three kinds of sensors, thermometer, anemometer and solar radiation sensor, are used to measure outside temperature, wind speed, and the intensity of solar radiation, respectively. A thermostat receives the signals from the sensors and controls the magnitude of electric voltage supplied to the TE units and the fans, as shown in Fig. 2. Under different weather conditions, the thermostat can adjust the power supplies to the designed optimal operating conditions.

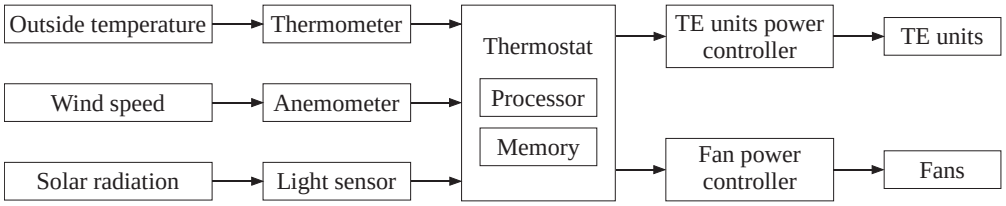

Figure 2. Thermostat and sensors

III. Optimization Problem of ATE Windows

III.A. Sampling Weather Conditions

The optimization of ATE windows design uses typical weather conditions in the US collected from the arranged climatic data through 2008.[26] The conditions include atmospheric temperature, wind speed, and solar radiation. The range of outside temperatures used in the optimization is 7 to $97°F$ (-14 to $36°C$ or 259 to $309K$). The maximum wind speed used is $21.5m/s$,[26] and the lowest is 0. In clear days, the maximum solar insolation on a surface perpendicular to incoming solar radiation is $1000W/m^2$. This value is used as the highest solar radiation and the lowest is 0.

The indoor temperature is maintained at $75°F$ ($24°C$ or $297K$) and the heat transfer coefficient is $3.6W/m^2$, which represent standard testing conditions for windows.[27]

To develop a surrogate model to evaluate optimal power supplies under different weather condition within the above ranges, the ATE window design needs to be optimized under a set of combinations of the weather conditions. The number of weather conditions used here is the small set population size defined by Colaco et al., which is equal to ten times the number of variables.[28] These sample combinations of weather conditions are generated using Sobol's Quasirandom sequence generator algorithm.[29] Thirty sample combinations of weather conditions are generated and are used for the optimization in Section III.B to develop surrogate models. To test the surrogate model, ten more sample combinations are generated.

III.B. Optimization Models

The design objective of ATE windows is to reduce the heat transfer through the building envelope with the least electric power consumption. The objectives of the optimization include (i) the minimization of the heat exchange between the air inside a room and outside, and (ii) the minimization of electric power consumption.

From the optimal results obtained in Section III, the total power consumption of fans is observed to be less than 6% of TE units power consumption. Therefore, the power consumption of the fans is not set as an objective.

The design variable is the electric voltage applied on the TE units, V_{te}, the average pressure gradient of the fans, Δp_{avg}, and the fan pressure gradient slope, k. The weather conditions, including outside temperature, T_{out}, wind speed, v_{wind}, and solar radiation, E_{solar}, are parameters for optimization. For each set of weather condition, optimization is performed, and the optimal values of V_{te}, Δp_{avg} and k are evaluated.

The amount of heat transfer is constrained by the operational envelope of the TE units. The dimensions of the side channels limit the number of TE units installed inside them. The conservation of energy through the ATE window system is modeled as equality constraints.

For ATI window, we define two optimization problems, one for cooling conditions and the other for heating conditions. The one for cooling conditions can be written as

$$\min_x f(x) = w_1 \dot{Q}_{in}^2 + w_2 P_{TE}^2 \tag{1}$$

$$x = \{V_{te}, \Delta p_{avg}, k\}$$

such that

$$-8 \leq \Delta p_{avg} \leq 8 \tag{2}$$

$$-0.1 \leq k \leq 0.1 \tag{3}$$

$$N_{te} A_{te} \leq A_{channel} \tag{4}$$

$$I_{te} \leq I_{max} \tag{5}$$

$$\Delta T_{te} \leq \Delta T_{max} \tag{6}$$

$$\dot{Q}_{cold} = \dot{Q}_{channel} \tag{7}$$

$$\dot{Q}_{hot} = \dot{Q}_{hs} \tag{8}$$

Similarly, the optimization for heating conditions is defined as

$$\min_x f(x) = w_1 \dot{Q}_{in}^2 + w_2 P_{TE}^2 \tag{9}$$

$$x = \{V_{te}, \Delta p_{avg}, k\}$$

such that

$$-8 \leq \Delta p_{avg} \leq 8 \tag{10}$$

$$-0.1 \leq k \leq 0.1 \tag{11}$$

$$N_{te} A_{te} \leq A_{channel} \tag{12}$$

$$I_{te} \leq I_{max} \tag{13}$$

$$\Delta T_{te} \leq \Delta T_{max} \tag{14}$$

$$\dot{Q}_{hot} = \dot{Q}_{channel} \tag{15}$$

$$\dot{Q}_{cold} = \dot{Q}_{hs} \tag{16}$$

where $\dot{Q}_{ATE}$ is the heat transferred through the inner pane; P_{TE} is the electric power consumed by the TE units; w_1 and w_2 are the weights for $\dot{Q}_{in}$ and P_{TE}; N_{te} is the number of the TE units; A_{te} is the area of one TE unit installed on the channels; $A_{channel}$ is the available area of the side channels; I_{te} is the electric current of the TE units; I_{max} is the maximum allowable electric current of TE units; ΔT_{te} is the temperature difference across the thermocouple; ΔT_{max} is the maximum allowable temperature difference across the thermocouple; $\dot{Q}_{hot}$ is the heat released from the hot side of the TE unit; $\dot{Q}_{cold}$ is the heat absorbed by the cold side of the TE unit; $\dot{Q}_{hs}$ is the heat transferred through the heat sink; and $\dot{Q}_{channel}$ is the heat exchange of the air flow in the channels.

III.C. Optimal Results

In Section III, the optimization is performed under the forty sets of weather conditions. Thirty of them are used as training data for surrogate models, and the other ten are used as testing data. The thirty sets of training data are listed in Table 4, and the other ten are listed in Table 12. The columns are (1) the weather

condition numbers, (2) the outside temperatures, T_{out}, (3) the wind speeds, v_{wind}, (4) the solar radiation, E_{solar}, (5) the absolute value of the optimal voltages supplied to TE units, V_{TE}, (6) the electric power of TE units, P_{TE}, (7) the average pressure gradient over one fan, Δp_{avg}, and (8) the pressure gradient slope, k. The bold outside temperatures are higher than the indoor temperature, $75°F$ $(297K)$, and these weather conditions (5, 8, 11, 16, 18, 21, 24, and 28) are cooling conditions.

IV. Surrogate Models of Optimal Operation

Since ATI windows are used under the wide range of weather conditions mentioned in Sec. III.A, they need to adjust the power supplies accordingly to achieve optimal performances. However, the computational expense of optimization under different weather conditions within the given range is excessive. Four surrogate modeling methods are used to approximate optimal power supplies under different weather conditions. The inputs of the surrogate models are weather condition parameters, including outside temperatures, T_{out}, wind speeds, v_{wind}, and solar radiation, E_{solar}. The ranges of the three inputs are 259 to $309K$, 0 to $21.5m/s$, and 0 to $1000W/m^2$, respectively. The outputs of the surrogate models include the the absolute value of the optimal voltages supplied to TE units, V_{TE}, the average pressure gradient over one fan, Δp_{avg}, and the pressure gradient slope, k.

In order to effectively account for the effects of the three inputs on the optimal results, the three inputs should be normalized. In the case of Kriging, the Dace Matlab Kriging Toolbox used in this paper performs the normalization by itself.[30] The normalization of the three inputs for the QRSM method, the RBF method and the E-RBF method are as follows.

$$\bar{T}_{out} = \frac{T_{out} - 259}{309 - 259} \tag{17}$$

$$\bar{v}_{wind} = \frac{v_{wind} - 0}{21.5 - 0} \tag{18}$$

$$\bar{E}_{solar} = \frac{E_{solar} - 0}{1000 - 0} \tag{19}$$

since the ranges of the three outputs are not limited to the optimal results, the outputs are not normalized. Except the Kriging method, the pressure gradient slope, k, is scaled 100 times as

$$\bar{k} = k \times 100 \tag{20}$$

IV.A. Quadratic Response Surface Model

The polynomial response surface method is easy to implement, and it shows a global trend. In this paper, the Quadratic Response Surface Method (QRSM) is used to express the absolute value of the optimal voltages supplied to TE units, V_{TE}, the average pressure gradient over one fan, Δp_{avg}, and the pressure gradient slope, k. The three candidate functions are as follows.

$$V_{TE} = a_0 + a_1\bar{T}_{out} + a_2\bar{v}_{wind} + a_3\bar{E}_{solar} + a_{12}\bar{T}_{out}\bar{v}_{wind}$$

$$+a_{13}\bar{T}_{out}\bar{E}_{solar} + a_{23}\bar{v}_{wind}\bar{E}_{solar} + a_{11}\bar{T}^2_{out} + a_{22}\bar{v}^2_{wind} + a_{33}\bar{E}^2_{solar} \tag{21}$$

$$\Delta p_{avg} = b_0 + b_1\bar{T}_{out} + b_2\bar{v}_{wind} + b_3\bar{E}_{solar} + b_{12}\bar{T}_{out}\bar{v}_{wind}$$

$$+b_{13}\bar{T}_{out}\bar{E}_{solar} + b_{23}\bar{v}_{wind}\bar{E}_{solar} + b_{11}\bar{T}^2_{out} + b_{22}\bar{v}^2_{wind} + b_{33}\bar{E}^2_{solar} \tag{22}$$

$$\bar{k} = c_0 + c_1\bar{T}_{out} + c_2\bar{v}_{wind} + c_3\bar{E}_{solar} + c_{12}\bar{T}_{out}\bar{v}_{wind}$$

$$+c_{13}\bar{T}_{out}\bar{E}_{solar} + c_{23}\bar{v}_{wind}\bar{E}_{solar} + c_{11}\bar{T}^2_{out} + c_{22}\bar{v}^2_{wind} + c_{33}\bar{E}^2_{solar} \tag{23}$$

In the above Eqs. (21), (22) and (23),the a_i's, b_i's, and c_i's, are coefficients determined by the least squares approach using the data normalized from Table 4. The values of the coefficients are listed in Table 5.

IV.B. Radial Basis Functions

The RBF method expresses surrogate models as linear combinations of simple basis functions. The basis functions are based on Euclidean distance.[1] Different types of parametric functions can be selected as bases. The Euclidean distance can be expressed as

$$r = \|x - x_i\| \tag{24}$$

where x_i is a sample point; and x is the variable.

In this paper, basis functions in the multiquadric form is used as the bases, which can be expressed as [1]

$$\psi(r) = (r^2 + \sigma_2)^{1/2} \tag{25}$$

where where $\sigma > 0$ is a user-defined parameter.

The approximation function is a weighted sum of the basis functions across all sample points, which is given by

$$\tilde{f}(x) = \sum_{i=1}^{n} \omega_i \psi(r) \tag{26}$$

where ω_i are coefficients to be evaluated.

To develop the three surrogate models for the optimal operation of the ATI window, the output, $\tilde{f}(x)$, in Eq. (26) is substituted by V_{TE}, Δp_{avg} and $\bar{k}$, respectively. The normalized $\bar{T}_{out}$, $\bar{v}_{wind}$ and $\bar{E}_{solar}$ are three inputs. The parameter, σ is tuned to 0.01 to minimize the errors between testing data and the surrogate model outputs. The coefficients ω_i of the surrogate models of V_{TE}, Δp_{avg} and $\bar{k}$ corresponding to all conditions in Table 4 are listed in Table 7, 8 and 9, respectively.

IV.C. Extended Radial Basis Functions

The Extended Radial Basis Functions (E-RBF) are developed to combine both radial and Non-Radial Basis Functions (N-RBF), which is an extension from RBF.[9] The non-radial basis functions are functions of each individual coordinate instead of the Euclidean distance. The N-RBF of the j^{th} dimension at the i^{th} sample point is expressed as [9]

$$\phi_{ij}(\xi_{ij}) = \alpha_{ij}^L \phi^L(\xi_{ij}) + \alpha_{ij}^R \phi^R(\xi_{ij}) + \beta_{ij} \phi^\beta(\xi_{ij}) \tag{27}$$

where ϕ^L, ϕ^R and ϕ^β are components of the N-RBFs; and α_{ij}^L, α_{ij}^R, and β_{ij} are coefficients to be evaluated. The definitions of α_{ij}^L, α_{ij}^R, and β_{ij} in different ranges are illustrated in Table 2.[9] In the table, γ is a user-defined parameter of design variable ranges.

Table 2. The definitions of coefficients for non-radial basis functions

Region	Range of ξ_j^i	ϕ^L	ϕ^R	ϕ^β
I	$\xi_j^i \le -\gamma$	$(-n\gamma^{n-1})\xi_j^i + \gamma^n(1-n)$	0	ξ_j^i
II	$-\gamma \le \xi_j^i \le 0$	$(\xi_j^i)^n$	0	ξ_j^i
III	$0 \le \xi_j^i \le \gamma$	0	$(\xi_j^i)^n$	ξ_j^i
IV	$\xi_j^i \ge \gamma$	0	$(n\gamma^{n-1})\xi_j^i + \gamma^n(1-n)$	ξ_j^i

The E-RBF functions are a linear combination of the RBFs and the N-RBFs. The combined function is expressed as [9]

$$\tilde{f}(x) = \sum_{i=1}^{n} \omega_i \psi(r) + \sum_{i=1}^{n} \sum_{j=1}^{m} \{\alpha_{ij}^L \phi^L(\xi_{ij}) + \alpha_{ij}^R \phi^R(\xi_{ij}) + \beta_{ij} \phi^\beta(\xi_{ij})\} \tag{28}$$

where n is the number of sample points; m is the number of design space dimensions; r is the Euclidean distance defined in Eq. (24); and ω_i are coefficients to be evaluated.

The output, $\tilde{f}(x)$, in Eq. (28) is substituted by V_{TE}, Δp_{avg} and $\bar{k}$, respectively for the three surrogate models. The normalized $\bar{T}_{out}$, $\bar{v}_{wind}$ and $\bar{E}_{solar}$ are three inputs. To minimize the errors between testing data and the surrogate model outputs, the parameter, σ, used in the RBFs is tuned to 0.01; and the parameter, γ, is tuned to 0.075. The coefficients for the surrogate models of V_{TE}, Δp_{avg} and $\bar{k}$ are listed in Table 7, 8 and 9, respectively.

IV.D. Kriging

The Kriging method estimates the summation of (i) a linear model and (ii) a systematic departure from the polynomial. The systematic departure stand for the fluctuations around the trend, which has a zero mean and a nonzero covariance. The general form of the kriging surrogate model can be expressed as[2]

$$\tilde{f}(x) = \mu + \varepsilon(x), E(\varepsilon) = 0, cov(\varepsilon(x_l), \varepsilon(x_k)) \neq 0, \forall l, k$$

A popularly used exponential correlation model is given by[2]

$$cov(\varepsilon(x_l), \varepsilon(x_k)) = \sigma^2 exp\left(- \sum_{m=1}^{N_{dv}} \phi_m (x_{l,m} - x_{k,m})^2 \right) \tag{29}$$

where N_{dv} denotes the number of the design space dimensions; σ is the standard deviation; ϕ_m is a measurement of the degree of correlation among the data along the m^{th} direction.

To develop surrogate models, second order ploynomial functions are used as regression models. The correlation between random output vectors are assumed as the exponential form in Eq. (29). The Matlab Kriging toolbox developed by Technical University of Denmark is used to determine the surrogate models.[30]

The correlation function parameter is 2. The generalized least squares estimate, β^*, for the three surrogate models are listed in Table 10. The correlation factors, γ^*, for three surrogate models are listed in Table 11. The estimates of process variance, σ^2, for three surrogate models, V_{TE}, Δp_{avg} and k, are 0.135, 0.229 and 0.00235, respectively.

V. Comparison of Surrogate Model Performance

The four types of surrogate models are developed in Section IV. Figures 3, 4, and 5 show the three output functions with respect to one of the input when the other two inputs are fixed at median values. The curves of four types of surrogate models are shown with specific colors in each figure. The values of the inputs and outputs in the figures are actual values, and are not normalized values.

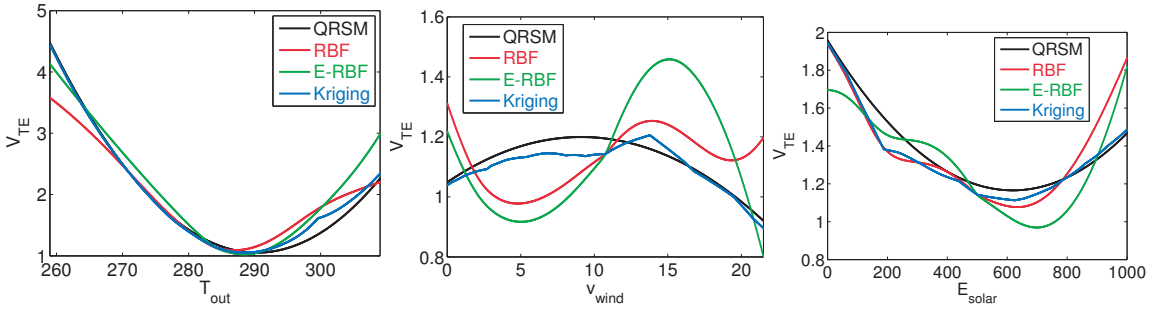

(a) V_{TE} vs T_{out} (b) V_{TE} vs v_{wind} (c) V_{TE} vs E_{solar}

Figure 3. V_{TE} **vs the three variables** T_{out}, v_{wind}, **and** E_{solar}

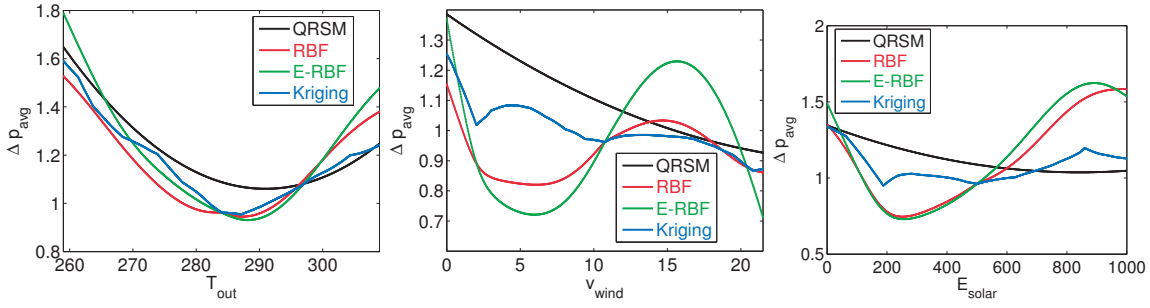

(a) Δp_{avg} vs T_{out} (b) Δp_{avg} vs v_{wind} (c) Δp_{avg} vs E_{solar}

Figure 4. Δp_{avg} **vs the three variables** T_{out}, v_{wind}, **and** E_{solar}

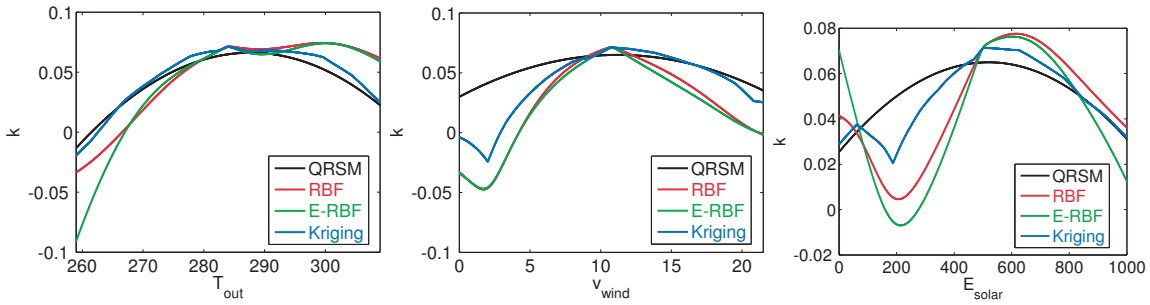

(a) k vs T_{out} (b) k vs v_{wind} (c) k vs E_{solar}

Figure 5. k vs the three variables T_{out}, v_{wind}, and E_{solar}

The overall performance of the surrogate models is evaluated by two standard accuracy measures: (i) Root Mean Squared Error (RMSE),[6,31] which provides a global error measure over the entire design domain, and (ii) Maximum Absolute Error (MAE),[10,32] which is indicative of local deviations. Ideally, it is desirable that both of these error measures are minimized. These metric measures are defined as

$$RMSE = \sqrt{\frac{1}{n_t}\sum_{k=1}^{n_t}\left(f(x^k) - \tilde{f}(x^k)\right)^2} \tag{30}$$

$$MAE = \max_k \left|f(x^k) - \tilde{f}(x^k)\right| \tag{31}$$

where $f(x^k)$ represents the actual function value for the test point x^k; $\tilde{f}(x^k)$ is the corresponding estimated value using the surrogate model; and n_t is the number of test points chosen for evaluating the error measure.

The 10 sets of testing data are listed in Table 12. The values of RMSE and MAE for different surrogate modeling methods are listed in Table 3. In each row, the smallest value corresponding to each function is highlighted with bold fonts.

Table 3. Performance comparison for different surrogate modeling methods

Output	Range	Metric	QRSM	RBF	E-RBF	Kriging
V_{TE}	2.9245	RMSE	0.3056 (10%)	**0.2754 (9%)**	0.4564 (16%)	0.2855 (10%)
		MAE	0.5623 (19%)	0.5669 (19%)	1.1492 (39%)	**0.5370 (18%)**
Δp_{avg}	2.2744	RMSE	**0.6132 (27%)**	0.6858 (30%)	0.7198 (32%)	0.6234 (27%)
		MAE	**1.2303 (54%)**	1.3257 (58%)	1.5004 (66%)	1.3247 (58%)
k	0.1587	RMSE	0.0534 (34%)	0.0341 (21%)	**0.0337 (21%)**	0.0548 (35%)
		MAE	0.0962 (61%)	**0.0578 (36%)**	0.0595 (37%)	0.0996 (63%)

The performance comparison in Table 3 shows that none of the surrogate modeling methods is universally superior to the other methods with respect to the current problem domain. For the three different outputs, particular methods are preferable to achieve higher accuracy. For V_{TE}, the performance of the RBF method and the Kriging method is better than that of the other two. For Δp_{avg}, the performance of the QRSM method and the Kriging method is better than that of the other two. For k, the performance of the RBF method and the E-RBF method is better than that of the other two.

Nevertheless, the performance metrics are dependent on the sampling method. If the testing points are different, the performance might be different. Hence, it would be more helpful to test sample points that represent typical environmental conditions.

Table 3 shows that the surrogate modeling method that has the lowest RMSE might not have the lowest MAE. In a region local to the sample point, the surrogate model with the lowest local errors is generally to be the best choice. For example, RBF has the lowest RMSE for V_{TE}. However, it does not have the lowest value of MAE for V_{TE}. It shows that, in certain regions in the weather condition space, RBF does not have the lowest errors.

A smart sampling method might be the way to deal with this issue. In this approach, the whole domain is divided into appropriate regions, and the space is sampled accordingly. To this end, a Latin hypercube sampling method can be implemented. Sequentially, the surrogate models are evaluated in the different regions; and the surrogate model that is locally more accurate than the others is selected. This method primarily separates the regions for implementation of the set of characteristically different surrogate models, in order to maintain a high accuracy over the whole domain.

VI. Concluding Remarks

To represent the optimal operation of the ATE window under varying environmental conditions, four types of surrogate models are developed, and their performances are compared. Quadratic Response Surface Methodology, Radial Basis Functions, Extended Radial Basis Functions, and Kriging are used. The parameters of the four types of surrogate models are determined. The performance comparison shows that the values of the two performance metrics, Root Mean Squared Error and Maximum Absolute Error, are at the same order of magnitude. None of the surrogate modeling methods has an overall better performance than the others in accuracy for the problem presented in this paper. For the different outputs of the optimal operation, particular methods have higher accuracy than the others, and hence are preferable to represent the optimal operation.

Acknowledgements

Support from the National Found Awards CMMI-0533330, and CMII-0946765 is gratefully acknowledged.

References

[1]Forrester, A. I. J., Sbester, A., and Keane, A. J., *Engineering Design via Surrogate Modelling: A Practical Guide*, Wiley, 1st ed., 2008.

[2]Queipo, N. V., Haftka, R. T., Shyy, W., Goel, T., Vaidyanathan, R., and Tucker, P. K., "Surrogate-based analysis and optimization," *Progress in aerospace sciences*, Vol. 41, 2005, pp. 1C28.

[3]Simpson, T. W., V. Toropov, V. B., and Viana, F. A. C., "Design and analysis of computer experiments in multidisciplinary design optimization: a review of how we have come - or not," 12*th AIAA/ISSMO Multidisciplinary Analysis and Optimization Conference*, Victoria, British Colombia, Canada, September 2008.

[4]Hosder, S., Watson, L. T., Grossman, B., Mason, W. H., Kim, H., Haftka, R. T., and Cox, S. E., "Polynomial Response Surface Approximations for the Multidisciplinary Design Optimization of a High Speed Civil Transport," *Optimization and Engineering*, Vol. 2, 2001, pp. 431C452.

[5]Hardy, R. L., "Multiquadric Equations of Topography and Other Irregular Surfaces," *Journal of Geophysical Research*, Vol. 76, 1971, pp. 1905–1915.

[6]Jin, R., Chen, W., and Simpson, T., "Comparative Studies of Metamodelling Techniques Under Multiple Modelling Criteria," *Structural and Multidisciplinary Optimization*, Vol. 23, No. 1, 2001, pp. 1–13.

[7]Cherrie, J. B., Beatson, R. K., and Newsam, G. N., "Fast Evaluation of Radial Basis Functions: Methods for Generalized Multiquadrics in R^n," *SIAM Journal of Scientific Computing*, Vol. 23, No. 5, 2002, pp. 1549–1571.

[8]Hussain, M. F., Barton, R. R., and Joshi, S. B., "Metamodeling: Radial Basis Functions, Versus Polynomials," *European Journal of Operational Research*, Vol. 138, No. 1, 2002, pp. 142–154.

[9]Mullur, A. A. and Messac, A., "Extended Radial Basis Functions: More Flexible and Effective Metamodeling," *AIAA Journal*, Vol. 43, No. 6, 2005, pp. 1306–1315.

[10]Mullur, A. A. and Messac, A., "Metamodeling Using Extended Radial Basis Functions: A Comparative Approach," *Engineering with Computers*, Vol. 21, No. 3, 2006, pp. 203–217.

[11]Zhang, J., Chowdhury, S., Messac, A., Castillo, L., and Lebron, J., "Response Surface Based Cost Model for Onshore Wind Farms Using Extended Radial Basis Functions," *ASME 2010 International Design Engineering Technical Conferences (IDETC)*, Montreal, Canada, August 15-18 2010.

[12]Giunta, A. and Watson, L., "A Comparison of Approximation Modeling Techniques: Polynomial Versus Interpolating Models," Tech. Rep. AIAA-98-4758, 1998.

[13]Sakata, S., Ashida, F., and Zako, M., "Structural Optimization Using Kriging Approximation," *Computer Methods in Applied Mechanics and Engineering*, Vol. 192, No. 7-8, 2003, pp. 923–939.

[14]Cressie, N., *Statistics for Spatial Data*, Wiley, New York, 1993.

[15]Duda, R., Hart, P., and Stork, D., *Pattern Classification*, Wiley-Interscience, 2nd ed., 2000.

[16]Yegnanarayana, B., *Artificial Neural Networks*, PHI Learning Pvt. Ltd., 2004.

[17]Clarke, S., Griebsch, J., and Simpson, T., "Analysis of Support Vector Regression for Approximation of Complex Engineering Analyses," *Journal of Mechanical Design*, Vol. 127, No. 6, 2005, pp. 1077–1087.

[18]Vapnik, V., *The Nature of Statistical Learning Theory*, Springer, New York, 1995.

[19]Basudhar, A. and Missoum, S., "Adaptive Explicit Decision Functions for Probabilistic Design and Optimization Using Support Vector Machines," *Computers and Structures*, Vol. 86, No. 19-20, 2008, pp. 1904–1917.

[20]Birthwright, R.-S., Messac, A., Harren-Lewis, T., and Rangavahala, S., "Heat Compensation in Buildings using Thermoelectric Windows: An Energy Efficient Window Technology," , No. DETC2008-50068, August 2008.

[21]Messac, A., Birthwright, R.-S., van Dessel, S., Khire, R., and Rangavahala, S., "Optimization-based Design of Active Thermal Insulator: An Energy Efficient Window," 7^{th} *World Congress of Structural and Multidisciplinary Optimization*, Seoul, Korea, May 2007.

[22]Messac, A., Birthright, R.-S., Harren-Lewis, T., and Rangavajhala, S., "Optimizing Thermoelectric Cascades to Increase The Efficiency of Thermoelectric Windows," 4^{th} *AIAA Multidisciplinary Design Optimization Specialist Conference*, Schaumburg, IL, April 2008.

[23]Harren-Lewis, T., Messac, A., Zhang, J., and Rangavajhala, S., "Multidisciplinary Design Optimization of Energy Efficient Side-Channel Windows," 5^{th} *AIAA Multidisciplinary Design Optimization Specialist Conference*, AIAA, Palm Springs, CA, May 2009.

[24]Zhang, J., Messac, A., Chowdhury, S., and Zhang, J., "Adaptive Optimal Design of Active Thermally Insulated Windows Using Surrogate Modeling," 51^{st} *AIAA/ASME/ASCE/AHS/ASC Structures, Structural Dynamics, and Materials Conference*, No. AIAA 2010-2917, AIAA, Orlando, Florida, April 2010.

[25]Rowe, D. M., *Thermoelectrics Handbook: Macro to Nano*, CRC PrI LIC, 2006.

[26]"Comparative Climatic Data for the United States through 2008," Tech. rep., http://www.noaa.gov.

[27]Mitchel, R., Kohler, C., Arasteh, D., Carmody, J., Huizeng, C., and Curcija, D., "Therm 5/Windows NFRC Simulation Manual," Tech. rep., Lawrence Berkeley National Laboratory, June 2003.

[28]Colaco, M. J., Dulikravich, G. S., and Sahoo, D., "A response surface method-based hybrid optimizer," *Inverse Probl Sci Eng*, Vol. 6, No. 16, 2008, pp. 717–741.

[29]Sobol, I. M., "Uniformly Distributed Sequences with an Additional Uniform Property," *USSR Computational Mathematics and Mathematical Physics*, Vol. 16, 1976, pp. 236–242.

[30]"DACE: A Matlab Kriging Toolbox," Tech. rep., http://www2.imm.dtu.dk/ hbn/dace/.

[31]Forrester, A. and Keane, A., "Recent Advances in Surrogate-based Optimization," *Progress in Aerospace Sciences*, Vol. 45, No. 1-3, 2009, pp. 50–79.

[32]Queipo, N., Haftka, R., Shyy, W., Goel, T., Vaidyanathan, R., and Tucker, P., "Surrogate-based Analysis and Optimization," *Progress in Aerospace Sciences*, Vol. 41, No. 1, 2005, pp. 1–28.

Appendix

Table 4. Training data of surrogate models

No.	T_{out}		v_{wind}	E_{solar}	V_{TE}	P_{TE}	Δp_{avg}	k
	(° F)	(K)	(m/s)	(W/m^2)	(V)	(W)	(Pa)	
1	52	284	10.75	500	1.14	0.97	0.96	0.071
2	74	297	5.38	750	0.97	2.96	0.95	0.067
3	29	272	16.13	250	3.28	9.88	1.77	0.019
4	40	278	8.06	625	1.34	1.17	1.00	0.079
5	**85**	**303**	18.81	125	1.00	2.42	1.16	0.069
6	63	290	2.69	375	0.77	0.90	0.97	0.040
7	23	268	6.72	313	3.24	8.71	1.04	0.031
8	**91**	**306**	1.34	563	2.48	19.97	1.15	0.051
9	46	281	12.09	63	2.28	6.68	1.53	0.074
10	35	275	4.03	938	2.35	4.49	1.89	0.069
11	**80**	**300**	13.78	438	2.37	18.71	1.15	0.079
12	57	287	9.41	188	0.86	0.53	0.46	-0.043
13	12	262	20.16	688	3.20	7.87	0.36	-0.055
14	15	264	10.08	844	2.55	4.59	0.42	-0.047
15	60	289	20.83	344	0.75	0.42	0.57	-0.053
16	**82**	**301**	4.70	94	0.97	2.35	0.98	-0.079
17	49	282	2.02	469	1.17	0.96	0.90	-0.072
18	**94**	**307**	12.77	969	3.34	37.95	1.17	-0.051
19	26	270	18.14	219	3.28	9.53	1.96	0.066
20	21	267	3.36	531	2.60	5.12	1.61	0.061
21	**88**	**304**	8.73	281	1.67	8.95	1.64	0.055
22	43	279	19.48	781	1.49	1.44	1.21	0.079
23	32	273	6.05	156	2.73	6.25	1.27	0.079
24	**77**	**298**	16.80	656	0.50	1.00	1.42	0.069
25	54	286	0.67	906	1.34	5.92	1.19	0.067
26	11	261	5.71	609	3.42	9.37	2.63	-0.071
27	56	286	16.46	109	1.45	2.25	1.21	0.042
28	**78**	**299**	0.34	359	1.37	6.14	1.75	0.007
29	33	274	11.09	859	1.86	2.47	1.89	0.008
30	44	280	3.02	234	1.84	2.70	2.00	0.015

Table 5. The coefficients of the QRSM models

V_{TE}		Δp_{avg}		$\bar{k}$	
a_0	5.7089	b_0	2.5637	c_0	−12.3870
a_1	−12.7827	b_1	−2.9976	c_1	23.3209
a_2	2.1000	b_2	−0.8956	c_2	25.3599
a_3	−4.5365	b_3	−0.8528	c_3	22.1596
a_{12}	8.7046	b_{12}	1.4402	c_{12}	−24.1011
a_{13}	−0.8406	b_{13}	0.2723	c_{13}	−12.9313
a_{23}	2.0716	b_{23}	0.4334	c_{23}	−14.6596
a_{11}	−1.5024	b_{11}	1.1991	c_{11}	−0.6189
a_{22}	5.2210	b_{22}	1.1151	c_{22}	9.3258
a_{33}	−1.2728	b_{33}	−0.8702	c_{33}	−23.1858

Table 6. The coefficients of the RBF surrogate model for V_{TE}

No.	V_{TE}	Δp_{avg}	$\bar{k}$
1	0.4388	−0.3977	−9.7083
2	2.7961	0.4489	−4.9128
3	−2.8074	0.8943	29.7266
4	0.8789	1.4236	−23.8633
5	1.8789	0.1234	−16.7702
6	1.7478	1.8263	−40.1173
7	−2.2671	2.5698	8.9110
8	−3.0921	1.1727	−8.7245
9	−1.7584	−1.9869	−28.0229
10	−1.6476	−1.8585	−17.7705
11	−7.1257	0.0957	−10.2915
12	3.5525	3.9360	48.9744
13	−0.5920	2.5356	16.6232
14	1.3607	6.7434	8.8733
15	2.5750	2.4845	41.4635
16	2.1585	2.4722	35.1246
17	0.6204	2.0331	70.3143
18	−3.5153	0.7966	26.2052
19	−0.3130	−2.1379	−37.2407
20	1.3924	2.0828	−49.7038
21	−0.8840	−2.9512	−20.1342
22	0.9858	−0.8436	−30.1086
23	−0.1232	1.2612	−28.5476
24	5.5056	−1.3434	−11.4660
25	2.5807	1.2860	−7.1548
26	−2.1249	−6.6269	48.3207
27	1.1824	0.1485	−2.5796
28	0.7156	−2.7402	3.2947
29	0.1038	−5.0578	10.0050
30	−0.7302	−5.0188	−3.5044

Table 7. The coefficients of the E-RBF surrogate model for V_{TE}

No.	ω_i	$\alpha^L_{T_{out}}$	$\alpha^R_{T_{out}}$	$\beta_{T_{out}}$	$\alpha^L_{v_{wind}}$	$\alpha^R_{v_{wind}}$	$\beta_{v_{wind}}$	$\alpha^L_{E_{solar}}$	$\alpha^R_{E_{solar}}$	$\beta_{E_{solar}}$
1	0.8652	−0.5469	0.8304	−0.1310	0.3402	−0.4898	−0.0632	−0.4108	0.5004	0.0000
2	0.6679	0.1424	0.2019	−0.1123	−0.0429	−0.1430	−0.0819	−0.2397	0.3246	0.0187
3	−0.4880	0.0848	0.1285	−0.1497	−0.3017	0.1790	−0.0445	0.2279	−0.1429	−0.0187
4	0.0286	−0.2441	0.4937	−0.1404	0.0400	−0.2066	−0.0725	−0.4827	0.5711	0.0094
5	0.8742	0.3179	0.0534	−0.1030	−0.1341	0.0213	−0.0351	0.0536	0.0255	−0.0280
6	0.5798	−0.2232	0.5383	−0.1217	−0.0187	−0.1889	−0.0912	0.0412	0.0473	−0.0093
7	−0.8111	0.1211	0.0732	−0.1544	−0.0344	−0.1416	−0.0772	0.1912	−0.1042	−0.0140
8	−0.9421	0.3788	0.0051	−0.0983	−0.0035	−0.2157	−0.0959	−0.4747	0.5641	0.0047
9	−1.8321	−0.4685	0.7353	−0.1357	0.2610	−0.4030	−0.0585	0	0.0754	−0.0327
10	−0.6657	−0.0400	0.2717	−0.1450	−0.0289	−0.1675	−0.0865	0.0703	0.0051	0.0327
11	−5.5114	0.2673	0.0907	−0.1077	−0.0625	−0.0708	−0.0526	−0.2041	0.2935	−0.0047
12	2.7211	−0.4203	0.7199	−0.1264	0.2065	−0.3644	−0.0678	0.1712	−0.0889	−0.0233
13	−0.5326	0.0032	0.1513	−0.1637	−0.1099	0.0012	−0.0305	−0.3705	0.4575	0.0140
14	3.2630	0.0296	0.1351	−0.1614	0.2927	−0.4463	−0.0655	−0.0518	0.1326	0.0257
15	−0.3050	−0.3211	0.6285	−0.1240	−0.1068	0	−0.0281	0.1281	−0.0403	−0.0117
16	1.3420	0.2878	0.0769	−0.1053	−0.0378	−0.1533	−0.0842	0.0137	0.0636	−0.0304
17	0.3860	−0.5366	0.8118	−0.1334	−0.0114	−0.2019	−0.0935	−0.3296	0.4192	−0.0023
18	−1.0265	0.3899	0	−0.0960	0.1497	−0.2881	−0.0562	0.0732	0	0.0351
19	−0.7541	0.1126	0.0912	−0.1521	−0.1660	0.0509	−0.0375	0.2150	−0.1313	−0.0210
20	2.0118	0.1034	0.0812	−0.1567	−0.0240	−0.1779	−0.0889	−0.4526	0.5421	0.0024
21	1.4873	0.3530	0.0247	−0.1007	0.1135	−0.2756	−0.0702	0.2231	−0.1371	−0.0163
22	−1.2108	−0.3593	0.6176	−0.1380	−0.1163	0.0057	−0.0328	−0.1788	0.2625	0.0210
23	0.2792	0.0363	0.1863	−0.1474	−0.0450	−0.1358	−0.0795	0.1099	−0.0291	−0.0257
24	3.8325	0.2224	0.1289	−0.1100	−0.2622	0.1422	−0.0421	−0.4378	0.5256	0.0117
25	1.2455	−0.5045	0.7961	−0.1287	0.0002	−0.2254	−0.0982	0.0492	0.0281	0.0304
26	−0.8726	0	0.1494	−0.1649	−0.0451	−0.1382	−0.0807	−0.4883	0.5771	0.0082
27	0.0301	−0.4666	0.7622	−0.1275	−0.2872	0.1659	−0.0433	0.0307	0.0475	−0.0292
28	0.0679	0.2523	0.1024	−0.1088	0	−0.2284	−0.0994	0.0874	0.0008	−0.0105
29	0.3892	0.0020	0.2252	−0.1462	0.3424	−0.4900	−0.0620	−0.0198	0.0997	0.0269
30	−1.0256	−0.4164	0.6790	−0.1369	−0.0223	−0.1824	−0.0900	0.2243	−0.1399	−0.0198

Table 8. The coefficients of the E-RBF surrogate model for p_{avg}

No.	ω_i	$\alpha^L_{T_{out}}$	$\alpha^R_{T_{out}}$	$\beta_{T_{out}}$	$\alpha^L_{v_{wind}}$	$\alpha^R_{v_{wind}}$	$\beta_{v_{wind}}$	$\alpha^L_{E_{solar}}$	$\alpha^R_{E_{solar}}$	$\beta_{E_{solar}}$
1	−0.0923	−0.4606	0.4517	−0.0254	0.2656	−0.4262	−0.0151	−0.1430	0.0124	−0.1647
2	−0.0996	−0.0458	0.0511	−0.0316	0.0235	−0.1901	−0.0089	−0.1751	0.1283	−0.1709
3	0.0599	0.5453	−0.5653	−0.0191	0.0691	−0.2206	−0.0213	−0.1283	−0.0832	−0.1584
4	1.5928	0.0698	−0.0847	−0.0222	0.0230	−0.1869	−0.0120	−0.0868	−0.0024	−0.1678
5	0.1157	0.0334	−0.0198	−0.0347	−0.0828	−0.0629	−0.0244	0.0366	−0.2872	−0.1553
6	1.0553	−0.2603	0.2582	−0.0285	0.0702	−0.2386	−0.0058	−0.3542	0.1828	−0.1616
7	2.7135	0.4946	−0.5169	−0.0176	−0.0361	−0.1293	−0.0104	−0.3054	0.1138	−0.1600
8	1.0342	0.0195	−0.0014	−0.0362	0.0237	−0.1927	−0.0042	−0.0248	−0.0852	−0.1662
9	−0.7943	−0.2692	0.2573	−0.0238	0.1946	−0.3532	−0.0167	0	−0.2700	−0.1538
10	−2.2448	0.3624	−0.3799	−0.0207	0.0660	−0.2336	−0.0073	0.0196	−0.0014	−0.1755
11	0.6636	−0.0120	0.0214	−0.0331	0.1190	−0.2748	−0.0186	−0.2851	0.1339	−0.1631
12	3.2732	−0.4203	0.4147	−0.0269	0.1369	−0.2993	−0.0135	0.0400	−0.2712	−0.1569
13	1.2699	0.0118	−0.0381	−0.0145	−0.1365	−0.0061	−0.0260	−0.1625	0.0944	−0.1693
14	6.2531	0.1034	−0.1288	−0.0152	0.2216	−0.3832	−0.0143	−0.0667	0.0522	−0.1732
15	1.5682	−0.3430	0.3391	−0.0277	−0.1410	0	−0.0268	−0.3424	0.1609	−0.1608
16	3.2998	0.0150	−0.0035	−0.0339	0.0530	−0.2201	−0.0081	0.0135	−0.2739	−0.1546
17	2.6280	−0.3957	0.3852	−0.0246	0.0518	−0.2206	−0.0050	−0.2153	0.0743	−0.1639
18	−1.0151	0.0203	0	−0.0370	0.1532	−0.3107	−0.0174	0.0292	0	−0.1763
19	−1.3864	0.5497	−0.5708	−0.0184	−0.0366	−0.1106	−0.0236	−0.0197	−0.2016	−0.1577
20	2.4653	0.3797	−0.4031	−0.0168	0.0692	−0.2372	−0.0066	−0.0730	−0.0474	−0.1654
21	−2.7092	0.0280	−0.0122	−0.0355	0.0715	−0.2347	−0.0128	−0.2308	0.0293	−0.1592
22	−1.3648	−0.0923	0.0788	−0.0230	−0.1173	−0.0269	−0.0252	−0.1585	0.1225	−0.1717
23	2.2663	0.4862	−0.5050	−0.0199	−0.0260	−0.1400	−0.0097	0.0492	−0.2901	−0.1561
24	−1.5731	−0.0268	0.0341	−0.0323	0.0460	−0.1961	−0.0221	−0.1322	0.0536	−0.1685
25	1.2131	−0.4686	0.4613	−0.0261	0.0033	−0.1726	−0.0034	0.0027	0.0045	−0.1748
26	−6.3645	0	−0.0268	−0.0141	−0.0033	−0.1630	−0.0093	−0.0572	−0.0372	−0.1674
27	0.9172	−0.4504	0.4440	−0.0265	0.0594	−0.2102	−0.0217	0.0263	−0.2818	−0.1549
28	−1.5927	−0.0207	0.0290	−0.0327	0	−0.1694	−0.0031	−0.3519	0.1754	−0.1612
29	−4.2938	0.4311	−0.4492	−0.0203	0.2575	−0.4176	−0.0155	−0.0417	0.0325	−0.1736
30	−3.8403	−0.1822	0.1696	−0.0234	0.0698	−0.2381	−0.0062	−0.0723	−0.1441	−0.1581

Table 9. The coefficients of the E-RBF surrogate model for k

No.	ω_i	$\alpha^L_{T_{out}}$	$\alpha^R_{T_{out}}$	$\beta_{T_{out}}$	$\alpha^L_{v_{wind}}$	$\alpha^R_{v_{wind}}$	$\beta_{v_{wind}}$	$\alpha^L_{E_{solar}}$	$\alpha^R_{E_{solar}}$	$\beta_{E_{solar}}$
1	−15.8042	−5.6613	3.2549	−2.0726	0.7714	−1.4202	0.7527	3.0948	−1.8768	−0.4735
2	−7.6532	−2.0058	0.6867	−2.2766	−1.8737	1.6523	0.9567	2.8212	−1.3154	−0.6775
3	25.3880	−7.0678	3.6761	−1.8685	2.3951	−3.3692	0.5486	1.2758	−0.2435	−0.2695
4	−16.0653	−8.4990	5.5873	−1.9706	−0.1593	−0.2886	0.8547	2.9111	−1.5619	−0.5755
5	−10.5345	−0.4755	−0.2616	−2.3786	0.3330	−1.4315	0.4466	0.3493	0.6283	−0.1675
6	−43.6668	−2.3215	0.4460	−2.1746	−0.4407	0.4712	1.0587	1.7417	−0.6293	−0.3715
7	3.1077	−4.7462	1.1242	−1.8175	−0.7447	0.4069	0.9057	1.7097	−0.6405	−0.3205
8	−19.1040	−0.3790	−0.0576	−2.4296	−0.0409	0.2069	1.1097	2.8064	−1.5260	−0.5245
9	−11.1937	−8.1132	5.4510	−2.0216	1.1415	−1.8812	0.7017	0	0.9599	−0.1165
10	−10.0080	−8.0130	4.8581	−1.9195	−2.1864	2.0877	1.0077	1.8461	−0.0576	−0.8306
11	−17.4306	−1.2787	0.2474	−2.3276	1.5243	−2.3692	0.6376	1.8656	−0.7036	−0.4225
12	36.3649	−3.4163	1.2722	−2.1236	0.2279	−0.7794	0.8037	0.8011	0.2007	−0.2185
13	15.5763	−0.0630	−4.0007	−1.7155	−1.0012	−0.1500	0.3956	2.9569	−1.5326	−0.6265
14	1.1821	−0.6127	−3.3429	−1.7410	0.5501	−1.1511	0.7782	2.1416	−0.5016	−0.7541
15	34.1779	−2.5615	0.5510	−2.1491	−1.1751	0	0.3701	1.8501	−0.7601	−0.3460
16	40.5897	−0.8178	−0.0672	−2.3531	−2.2750	2.1141	0.9822	0.1330	0.8350	−0.1420
17	72.8430	−7.0252	4.4902	−2.0471	−0.0089	0.1064	1.0842	2.5419	−1.3527	−0.4480
18	9.7882	−0.2840	0	−2.4551	1.2563	−2.0390	0.6762	1.8413	0	−0.8561
19	−17.3603	−6.1109	2.6033	−1.8430	1.2893	−2.3591	0.4721	1.0415	−0.0253	−0.2440
20	−39.9814	−3.1712	−0.5636	−1.7920	−1.4469	1.4120	1.0332	3.0412	−1.7927	−0.4990
21	−27.5302	−0.3888	−0.1989	−2.4041	−0.0429	−0.4576	0.8292	1.5419	−0.4920	−0.2950
22	−19.0562	−8.5089	5.7212	−1.9961	−0.4801	−0.6456	0.4211	2.6007	−1.0517	−0.7031
23	−14.0699	−7.6322	4.3582	−1.8941	−1.2594	0.9790	0.9312	0.5239	0.4650	−0.1930
24	−14.5782	−1.6797	0.5038	−2.3021	2.4661	−3.4737	0.5231	2.9467	−1.5607	−0.6010
25	−17.5308	−4.5030	2.2270	−2.0981	−0.0112	0.2474	1.1352	1.9440	−0.2065	−0.8051
26	27.7169	0	−4.1171	−1.7028	−1.5660	1.3148	0.9440	2.8447	−1.5133	−0.5628
27	2.9759	−3.9590	1.7488	−2.1108	2.4920	−3.4831	0.5359	0.2531	0.7195	−0.1547
28	−6.5530	−1.4886	0.3848	−2.3149	0	0.2718	1.1480	1.8499	−0.7489	−0.3587
29	20.0199	−7.8445	4.6298	−1.9068	0.8933	−1.5654	0.7399	2.0854	−0.4216	−0.7668
30	0.9049	−8.3776	5.6524	−2.0088	−0.9299	0.9275	1.0460	1.1242	−0.1002	−0.2567

Table 10. The generalized least squares estimates of the Kriging surrogate models

V_{TE}	p_{avg}	k
$-7.617E-01$	$-3.025E-01$	$7.221E-01$
$-6.766E-01$	$-2.446E-01$	$1.706E-01$
$-8.635E-03$	$-2.942E-01$	$1.275E-01$
$-1.560E-01$	$-1.534E-01$	$1.184E-01$
$7.330E-01$	$1.880E-01$	$-3.572E-01$
$-1.321E-01$	$2.293E-01$	$-1.350E-02$
$4.345E-01$	$1.608E-01$	$1.282E-01$
$-8.715E-02$	$5.978E-02$	$-2.048E-01$
$-1.105E-01$	$-8.750E-02$	$-3.537E-01$
$1.731E-01$	$8.039E-02$	$-1.974E-01$

Table 11. The correlation factors of the Kriging surrogate model

V_{TE}	p_{avg}	k
$-5.937E-02$	$-1.321E-01$	$2.027E-01$
$-7.537E-01$	$-4.619E-01$	$6.387E-02$
$4.340E-01$	$6.239E-01$	$-7.076E-01$
$-1.797E-01$	$-4.705E-01$	$4.841E-01$
$-1.434E-01$	$-2.682E-01$	$8.289E-01$
$-3.001E-01$	$-5.707E-01$	$4.237E-01$
$1.934E-01$	$-1.116E+00$	$1.032E-01$
$2.878E-01$	$-1.443E-01$	$6.298E-01$
$1.813E-01$	$4.337E-01$	$6.936E-01$
$6.956E-01$	$8.539E-01$	$6.275E-01$
$1.316E+00$	$5.047E-02$	$5.017E-01$
$-5.363E-01$	$-1.480E+00$	$-1.678E+00$
$-1.454E-01$	$-1.055E+00$	$-1.367E-01$
$-3.904E-01$	$-2.012E+00$	$-4.874E-01$
$-1.448E-01$	$-9.488E-01$	$-1.920E+00$
$-3.187E-01$	$-3.483E-01$	$-9.905E-01$
$4.823E-03$	$-9.275E-01$	$-2.139E+00$
$6.499E-02$	$-4.579E-01$	$-1.055E+00$
$-1.841E-01$	$1.133E+00$	$7.124E-01$
$-1.097E-01$	$-3.331E-01$	$1.177E+00$
$1.563E-01$	$1.046E+00$	$7.649E-01$
$4.497E-01$	$7.835E-01$	$1.410E+00$
$-2.398E-02$	$-5.875E-01$	$1.295E+00$
$-8.193E-01$	$6.772E-01$	$5.383E-01$
$-1.756E-01$	$-5.218E-01$	$1.106E-01$
$-1.200E-01$	$1.902E+00$	$-1.219E+00$
$-7.386E-02$	$3.032E-02$	$-2.261E-01$
$2.125E-01$	$1.207E+00$	$9.903E-02$
$1.724E-01$	$1.820E+00$	$-2.789E-01$
$3.097E-01$	$1.275E+00$	$1.728E-01$

Table 12. Testing data for surrogate models

No.	T_{out} (K)	v_{wind} (m/s)	E_{solar} (W/m^2)	V_{TE} (V)	P_{TE} (W)	Δp_{avg} (Pa)	k
1	$2.934E+02$	$1.747E+01$	$8.125E+02$	$9.809E-01$	$1.159E+00$	$3.108E-02$	
2	$2.949E+02$	$7.391E+00$	$7.188E+02$	$1.030E+00$	$2.376E+00$	$6.829E-02$	
3	$2.926E+02$	$8.398E+00$	$9.844E+02$	$1.291E+00$	$1.446E+00$	$1.002E-02$	
4	$2.676E+02$	$1.915E+01$	$4.844E+02$	$2.995E+00$	$1.669E+00$	$1.253E-02$	
5	$3.082E+02$	$7.055E+00$	$4.688E+01$	$1.875E+00$	$1.947E+00$	$4.645E-02$	
6	$3.020E+02$	$2.049E+01$	$9.219E+02$	$2.210E+00$	$1.419E+00$	$1.352E-02$	
7	$2.879E+02$	$1.579E+01$	$7.656E+02$	$1.041E+00$	$1.505E+00$	$4.800E-02$	
8	$3.004E+02$	$1.041E+01$	$5.156E+02$	$1.337E+00$	$1.721E+00$	$4.850E-03$	
9	$2.817E+02$	$7.727E+00$	$8.906E+02$	$1.800E+00$	$9.036E-01$	$-2.726E-02$	
10	$2.910E+02$	$1.982E+01$	$5.781E+02$	$6.808E-01$	$4.238E-01$	$-4.826E-02$	